Journal of Structural Biology 187 (2014) 66–75

Contents lists available at ScienceDirect

Journal of Structural Biology

journal homepage: www.elsevier.com/locate/yjsbi

# Automated particle correspondence and accurate tilt-axis detection in tilted-image pairs

Maxim Shatsky [a,*,1], Pablo Arbelaez [b,1], Bong-Gyoon Han [c], Dieter Typke [c], Steven E. Brenner [a,d], Jitendra Malik [b], Robert M. Glaeser [c]

[a] Physical Biosciences Division, Lawrence Berkeley National Laboratory, CA 94720, USA
[b] Electrical Engineering and Computer Science Division, University of California, Berkeley, CA 94720, USA
[c] Life Sciences Division, Lawrence Berkeley National Laboratory, CA 94720, USA
[d] Department of Plant and Microbial Biology, University of California, Berkeley, CA 94720, USA

ARTICLE INFO

*Article history:*
Received 24 October 2013
Received in revised form 7 March 2014
Accepted 21 March 2014
Available online 30 March 2014

*Keywords:*
Particle correspondence
Tilted pairs
Tilt-axis detection

ABSTRACT

Tilted electron microscope images are routinely collected for an *ab initio* structure reconstruction as a part of the Random Conical Tilt (RCT) or Orthogonal Tilt Reconstruction (OTR) methods, as well as for various applications using the "free-hand" procedure. These procedures all require identification of particle pairs in two corresponding images as well as accurate estimation of the tilt-axis used to rotate the electron microscope (EM) grid. Here we present a computational approach, PCT (particle correspondence from tilted pairs), based on tilt-invariant context and projection matching that addresses both problems. The method benefits from treating the two problems as a single optimization task. It automatically finds corresponding particle pairs and accurately computes tilt-axis direction even in the cases when EM grid is not perfectly planar.



## 1. Introduction

The primary goal of single-particle cryo-electron microscopy (EM) is to obtain a three-dimensional (3D) reconstruction of a particle from its two-dimensional projections (Frank, 2006; Glaeser et al., 2006). *Ab initio* reconstruction methods from frozen samples have only shown limited success, and thus projection matching against a template volume currently is the most widely used approach. In cases when an initial model is not available, a low-to-medium resolution model can be obtained from negatively stained samples by the Random Conical Tilt (RCT) (Radermacher et al., 1986; Radermacher, 1988) or Orthogonal Tilt Reconstruction (OTR) (Leschziner and Nogales, 2006; Leschziner, 2010) procedures. RCT has also been applied to low-tilt cryo-EM samples of the 70S ribosome (Penczek et al., 1994), but this approach has not been widely used in further work.

In both the RCT and OTR approaches, two images of the same sample are collected. The computational processing steps for both methods are mostly equivalent. The geometry of the images has to be estimated, which includes tilt angle and tilt-axis direction (i.e., the direction of the goniometer relative to the recorded image). Next, particles are identified and boxed in both images, and the correspondence between the same particles is established. Then, particles from one image are used to compute class averages. Usually the largest cluster of similar projections is picked and its corresponding paired images are used to reconstruct a 3D model. To improve the quality of the model, reconstructions from several class averages can be merged (Penczek et al., 1994; Scheres et al., 2009).

A second use of tilt-pair images is to determine the absolute hand of a structure (Belnap et al., 1997; Cheng et al., 2002), improve the refinement of Euler angles, and reduce the tendency of the model to match noise. In the "free-hand" method introduced by Rosenthal and Henderson (2003) and Henderson et al. (2011), for example, projection matching is used to assign Euler angles to particle images obtained with an untilted specimen. An exhaustive search is then used to determine the amount and orientation of tilt for which corresponding projections of the current model agree best with a second image, obtained after tilting the specimen by +10°. Errors in the initial assignment of Euler angles affect how closely the search results agree with the known tilt angle, as set by the goniometer. A target function was thus constructed that used tilt-pair images to obtain improved assignments for the Euler

* Corresponding author. Address: 461 Koshland Hall, University of California, Berkeley, CA 94720-3102, USA.
*E-mail address:* max.shatsky@gmail.com (M. Shatsky).
[1] These authors contributed equally to this work.

http://dx.doi.org/10.1016/j.jsb.2014.03.017
1047-8477/

angles in each cycle of refinement (Rosenthal and Henderson, 2003). Although initially not widely adopted, the "free-hand" approach is gaining in use, and it is now available in various single-particle software packages (SPIDER: Shaikh et al., 2008; EMAN2: Tang et al., 2007).

The RCT, ORT and "free-hand" processes rely on accurate determination of corresponding particle pairs. While there are several packages that offer automated particle selection from a single micrograph (for a review and comparison see Arbeláez et al. (2011)), particle picking from a tilted pair of images is usually done by hand with a help of graphical interface like that in the XMIPP package (Scheres et al., 2008). Recently, an automated approach has been proposed that brings into correspondence particle pairs from a pair of tilted images (Hauer et al., 2013).

The magnitude of a tilt angle is a user-controlled parameter, and in practice it accurately corresponds with the resulting experimental value. What is usually left undetermined is the direction of the tilt-axis relative to micrographs of tilted and un-tilted specimens. This value can be determined from the geometry of the positions of the corresponding particles. Commonly used packages for determining the direction of tilt assume that the specimen is planar. Given this assumption and a set of identified corresponding particle-center pairs $\{v_i, u_i\}$, an affine transform can be computed that relates particle centers in both images: $v_i = s\,A\,u_i$, where $A$ is a rotational matrix and $s$ is a scaling vector which depends on the tilt angle. TiltPicker (Voss et al., 2009) optimizes least squares for this linear relation, and the tilt-axis directions of both images are extracted from $A$. TiltPicker adopts a semi-automated iterative approach to resolve the difficulty of computing the required parameters, i.e., tilt angles, shift and corresponding particle pairs. The XMIPP package (Scheres et al., 2008) assumes that one image is non-tilted. Given the corresponding particle pairs it essentially reconstructs 3D coordinates of the particles from the tilted-image. Again, the assumption is that the EM grid is flat. CTFTILT (Mindell and Grigorieff, 2003) is based on the assumption that the contrast transfer function (CTF) changes the least along the direction of the tilt-axis. Therefore, this approach also assumes that the EM grid is planar and there is no pre-tilt of the sample in a direction different from that of the goniometer. In practice, however, the deviations from these two assumptions could result in errors of several degrees for tilt-axis calculations. Consequently, errors in tilt-axis direction are expected to result (a) less accurate particle matching identification, if a method relies on tilt geometry like the presented PCT and the recently introduced MaverickTilt (Hauer et al., 2013) methods; and (b) wrong placement of images in Fourier space. Thus in both cases, the tilt-axis errors may impact the reconstruction quality. For microscopes based on film detectors the tilt-axis direction needs to be computed for every pair of tilted images, since the film can at least be slightly rotated when placed into a microscope and then when placed into a scanner. Such problems do not occur with CCD or DDD equipped detectors; however, direction of the tilt-axis changes with magnification and after a microscope is serviced.

In this work our goal is to give an accurate solution to finding both the particle correspondence and the tilt-axis estimation. For the first stage of particle picking in individual images we make use of the semi-automated TextonSVM method (Arbeláez et al., 2011), where the user selects a small set of characteristic particles that serve as exemplars, and their characteristic texture is used to train an SVM classifier. Here, we extend this approach to identify corresponding particle pairs from a pair of images of a tilted sample. The texture descriptors of TextonSVM are extended with tilt-invariant context descriptors. These new descriptors allow the identification of an initial correspondence between the particles as well as to find approximate tilt-axis angles. The correspondence and the tilt-axis angles are consequently refined using a method similar to a common-line comparison that relates two micrographs based on their 1D projections of particle centers. Using 1D projections allows us to avoid assumptions about EM grid planarity, and at the same time allows us to avoid a complex modeling of EM grid geometry. We have also developed a graphical interface that allows manual editing of selected particle pairs. In Section 5 we demonstrate the accuracy of our method, PCT (particle correspondence from tilted pairs), on three sets of experimentally produced images. In addition, using synthetic data, we show how reasonably expected geometrical deformations of EM grid affect tilt-axis estimates by the commonly used affine transform, while our approach gives robust results in the presence of these types of deformations.

## 2. Methods

### 2.1. Data acquisition

#### 2.1.1. Tilted projections of gold particles

The aim of the experiments described in the following was to test recording of tilt pairs on the JEOL SFF 3100 TEM. A home-made carbon film was used to which 10 nm gold particles had been applied. Tilt pairs were recorded at ±15° tilt angles, at 300 kV accelerating voltage, and 60,000× EM magnification. Images were recorded with a CCD camera. To minimize the displacement between the images of the tilt pair, the eucentric height was carefully adjusted. In order to determine the direction of the tilt-axis, additional images of the same area were recorded at 0°, 30°, and 60° tilt angles. For this paper we considered one series of five images recorded at −15°, 0°, 15°, 30° and 60°.

#### 2.1.2. Tilt pairs of inosine-5′-monophosphate dehydrogenase

Inosine-5′-monophosphate dehydrogenase (IMP dehydrogenase, YP_010265.1) with MW of 420 kDa was purified from *Desulfovibrio vulgaris* Hildenborough and negatively stained with Uranyl Acetate solution (Han et al., 2009). EM images were recorded on Kodak SO-163 film at a magnification of 40,000 with under focus values ranging from 1 to 2 μm on a JEOL 4000 microscope operated at 400 kV. Initially, the specimen stage was tilted to 45°, and images were collected by using low dose technique. Following this, the specimen stage was tilted back for the collection of images of untilted specimens from the same area. The exposure for each image was ~20 electrons/Å$^2$. A total of seven tilt-pair images were digitized with a resolution of 1.59 Å/pixel at the sample level.

#### 2.1.3. Tilted projections of Escherichia coli 70S ribosome particles

The samples were prepared using the same protocol as in (Han et al., 2009). The purified ribosome samples, a gift from the laboratory of Prof. Jamie Cate, were applied on a glow discharged holey carbon grid (Quanti foil). The grid was frozen in liquid ethane for cryo-electron microscopy, by using a Vitrobot operated at ambient temperature and 80% humidity. The cryo-EM images were recorded on Kodak SO-163 films at a magnification of 50,000× using a Philips CM200 TEM operated at 200 kV with under-focus values of 2–3 μm. A total of 34 tilt-pair images were recorded at ±15° using low-dose conditions with an exposure of ~15 electrons/Å$^2$ per image. The recorded images were digitized using the Nikon Super Coolscan 8000 ED densitometer, operated by a film scanning

robot (Typke et al., 2005). The images were scanned with a step size of 6.35 μm, resulting in a resolution of 1.27 Å/pixel.

*2.1.4. Synthetic data*

Synthetic pairs of images at 0° and 45° tilt were generated of 200 randomly placed points (to simulate particle centers) in images of 2K × 2K pixels. To allow noise in particle-center coordinates, a random number in the range of minus ten and ten is added to the $x$ and $y$ coordinates of particles in the second image. The threshold of ten is chosen to simulate the worst case of center misclassification in the case of a particle width equal to twenty pixels, as in the experimental images of *E. coli* 70S ribosome. Such a large displacement also may take into account possible particle displacement due to the beam induced movement which can reach 10 Å (Bai et al., 2013).

We generated four types of images designed to test different types of geometrical deformations of an EM grid. The first set assumed that the specimen is perfectly flat. The next three are for specimens that are curved according to the shapes of parabola, paraboloid and saddle, respectively (Fig. 1). The parabolic shape is modeled as $Z = \alpha\ (X - 1000)^2$, the paraboloid is modeled as $Z = \alpha\ ((X - 1000)^2 + (Y - 1000)^2)$, and the saddle is modeled as $Z = \alpha\ ((X - 1000)^2 - (Y - 1000)^2)$. We set $\alpha = 1/10{,}000$ so that in the case of a parabola the image corner rises by 100 pixels, which is 5.7° from the image center.

To test the effect of the beam-induced movement we constructed pairs of images by taking a flat image as the first one and then applying a parabolic deformation to it. The deformation is applied in such a way that the geodesic distances between the particles are preserved and the angle created by the vector going from the image center to the most elevated image edge is 4°.

## 3. Particle correspondence and tilt-axis detection

In the first step we apply a previously published particle-picking algorithm TextonSVM (Arbeláez et al., 2011) to each image (Box 1: lines 1.1–1.5). Given two sets of identified particles from two tilted images our goal is to establish a list of corresponding pairs. To find an initial correspondence we compare particle neighborhoods from two images. A neighborhood is roughly defined as a sub-image of size ten times the particle radius taken around the particle center. Unlike the whole micrograph, we do not expect local neighborhoods to have significant geometrical distortions. Thus, after appropriately shrinking one dimension of the sub-image by $1/\cos(\alpha_{\text{tilt}})$, where $\alpha_{\text{tilt}}$ is the given tilt angle relative to the absolute zero (i.e., the image plane), two neighborhoods of the same particle are going to be very similar. To have sub-images properly normalized and to increase robustness of the representation, the neighborhoods are defined as sub-images of the probability map that is computed by TextonSVM as a part of the particle-detection process. The probability map has the same dimensions as the original image, and each pixel has a value between zero and one, which represents the probability of observing a particle at this location (Box 1: lines 2.1–2.8).

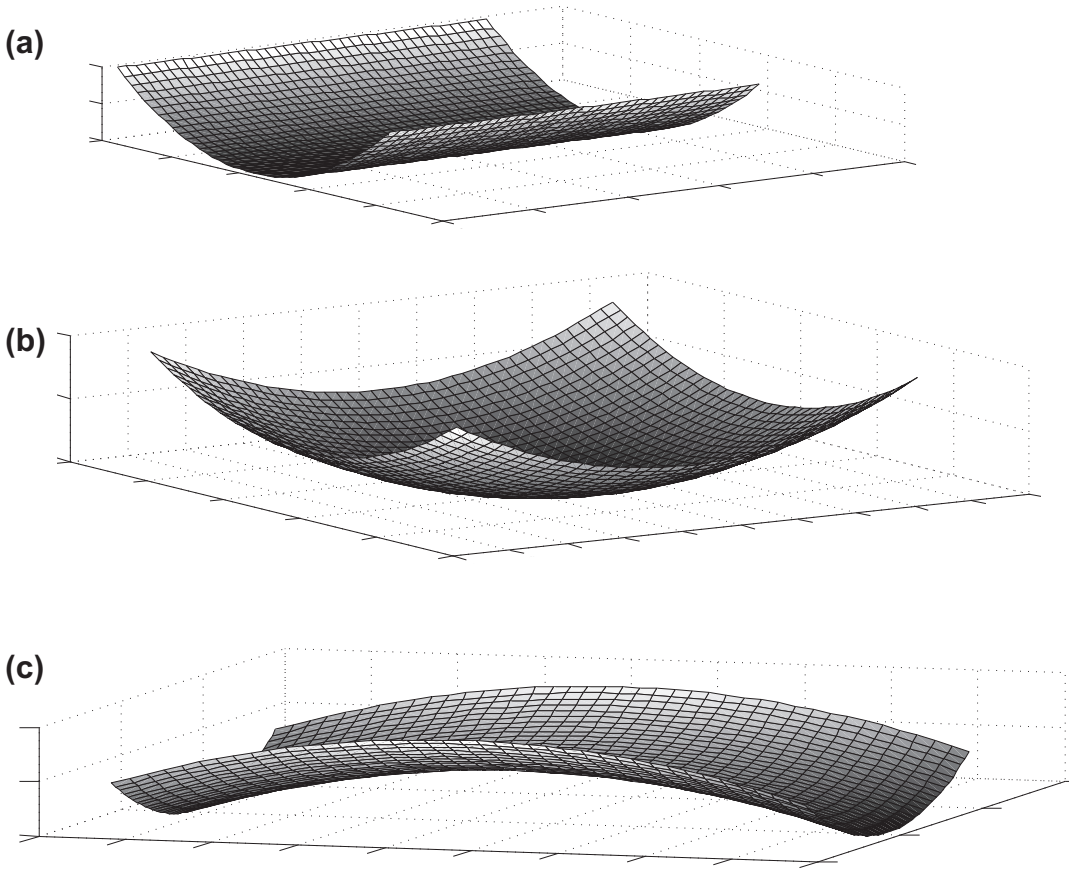


**Fig.1.** Examples of EM grid geometrical deformations. (a) Parabolic folding, (b) parabaloid and (c) saddle.

Box 1 Pseudo code of the PCT method.

1. Apply particle detection for each micrograph image (Arbeláez et al., 2011).
   1.1 For each image $I \in (I_1, I_2)$
   1.2 Apply TextonSVM to compute:
   1.3 a) probability map $PM(I)$
   1.4 b) particle centers $P(I) = \{v_i\}$
   1.5 End

2. Compute neighborhood descriptors.
   2.1 For each probability map $PM(I)$ of image $I \in (I_1, I_2)$
   2.2 For each angle $\phi \in (5, 10,\ldots, 360)$ ($\phi \in (5, 10,\ldots, 180)$ if $I \equiv I_2$)
   2.3 Compute stretched image along direction $\phi$: $I_\phi = Stretch(I, \phi, 1/\cos(\alpha_{tilt}))$, where *Stretch* changes image coordinates along direction $\phi$ by $1/\cos(\alpha_{tilt})$.
   2.4 For every particle $v_i \in P(I_\phi)$ compute a descriptor within a box of 40 × 40 Å:
   2.5 $h_{i,\phi} = I_\phi\,[v_{i,x} \pm 40$ Å$: v_{i,y} \pm 40$ Å$]$.
   2.6 End
   2.7 End
   2.8 End

3. Initial matching:
   3.1 For every pair of angles $(\phi_1, \phi_2) \in (1,\ldots, 360) \times (1,\ldots, 180)$
   3.2 Compute similarity between every pair of descriptors:
   $$s_{i,j} = 1 - \chi^2(h_{1,i,\phi_1}, h_{2,j,\phi_2})$$
   3.3 Find reciprocal best matches: $M(\phi_1, \phi_2) = \{i', j' : s_{i',j'} = \max_j\{s_{i',j}\} \wedge s_{i',j'} = \max_i\{s_{i,j'}\}\}$.
   3.4 Compute overall score: $S(\phi_1, \phi_2) = \sum_{i',j'} s_{i',j'}$.
   3.5 End
   3.6 Initial matching: $M(\phi_{max1}, \phi_{max2})$ such that
   $$(\phi_{max1}, \phi_{max2}) = \arg_{\phi_1,\phi_2} \max\{S(\phi_1, \phi_2)\}$$

4.1 D projection matching. Matching refinement and tilt-axis detection:
   4.1 For every pair of angles $(\alpha_1, \alpha_2) \in (1,\ldots, 360) \times (1,\ldots, 180)$
   4.2 Compute 1D projections from $M(\phi_{max1}, \phi_{max2})$:
   $(Proj_1(\alpha_1), Proj_2(\alpha_2))$.
   4.3 Compute histogram of coordinate differences between the matched particles:
   $H(\alpha_1, \alpha_2) = \{v_i - u_i : v_i \in Proj_1(\alpha_1), u_i \in Proj_2(\alpha_2)\}$.
   4.4 Find the height of the peak (1 pixel bins, 5 pixel window = half particle size), and corresponding particle pairs at the peak (a voting step):
   $$[h_{\alpha_1,\alpha_2}, \{i'\}_{\alpha_1,\alpha_2}] = Peak(H(\alpha_1, \alpha_2)).$$
   4.5 End
   4.6 Select the best peak: $(\alpha_{max1}, \alpha_{max2}) = \arg_{\alpha_1,\alpha_2} \max\{h_{\alpha_1,\alpha_2}\}$
   4.7 Tilt-axis: $(\alpha_{max1}, \alpha_{max2})$
   4.8 Matched particles: $\{i'\}_{\alpha_{max1},\alpha_{max2}}$

### 3.1. Initial tilt direction and particle correspondence

In order to compare particles' neighborhoods we need to properly position them with the in-plane rotation. At this stage, however, we do not know the direction of the tilt-axis to define the correct orientation. Therefore, for one image we create a tilt-invariant context descriptor, which is a set of neighborhood descriptors for all 360°. We then exhaustively iterate over all pairs of potential tilt-axis directions $(\phi_1, \phi_2) \in (5, 10,\ldots, 360) \times (5, 10,\ldots,180)$ and compute the similarity between all pairs of neighborhoods. We then pick corresponding pairs based on the best reciprocal scores, $i$ picks $j$ if $i$ is most similar to $j$ and vice versa. Each pair of angles $(\phi_1, \phi_2)$ defines the sum of reciprocal scores. The highest scoring pair of angles defines both the direction of the tilt and the initial correspondence (Box 1: lines 3.1–3.6).

### 3.2. 1D projection matching. Matching refinement and tilt-axis detection

Projection matching has been widely used in various EM applications (Frank, 2006; van Heel, 1987). A one-dimensional projection, or the Radon Transform in two-dimensional space, is a summation of 2D image voxels along a given direction. Any two EM images of the same volumetric sample obtained at different Euler angles have an identical (common) one-dimensional projection, also called a common line in Fourier space. The specimen tilt-axis exactly corresponds to the common line of two images of the specimen that are recorded at different tilt angles. Therefore, in order to accurately identify the direction of the tilt-axis in each of the two images we look for their common line by searching for the most similar pair of 1D projections. In this work, however, instead of using projections of the original 2D images, we define coordinate vectors of projected particle centers. This is depicted in Fig. 2. Once particles are identified in an image we compute their corresponding centers of mass. These particle centers are then projected onto a given line, thus, essentially creating a list of real value coordinates. Utilizing particle centers instead of all image pixels allows us to avoid dealing with problems of noise, varying contrast, and unequal distribution of rectangular image pixels under different angles. An additional benefit is that the number of particles is substantially smaller then the size of the image; thus, computing their 1D projections can be done extremely rapidly.

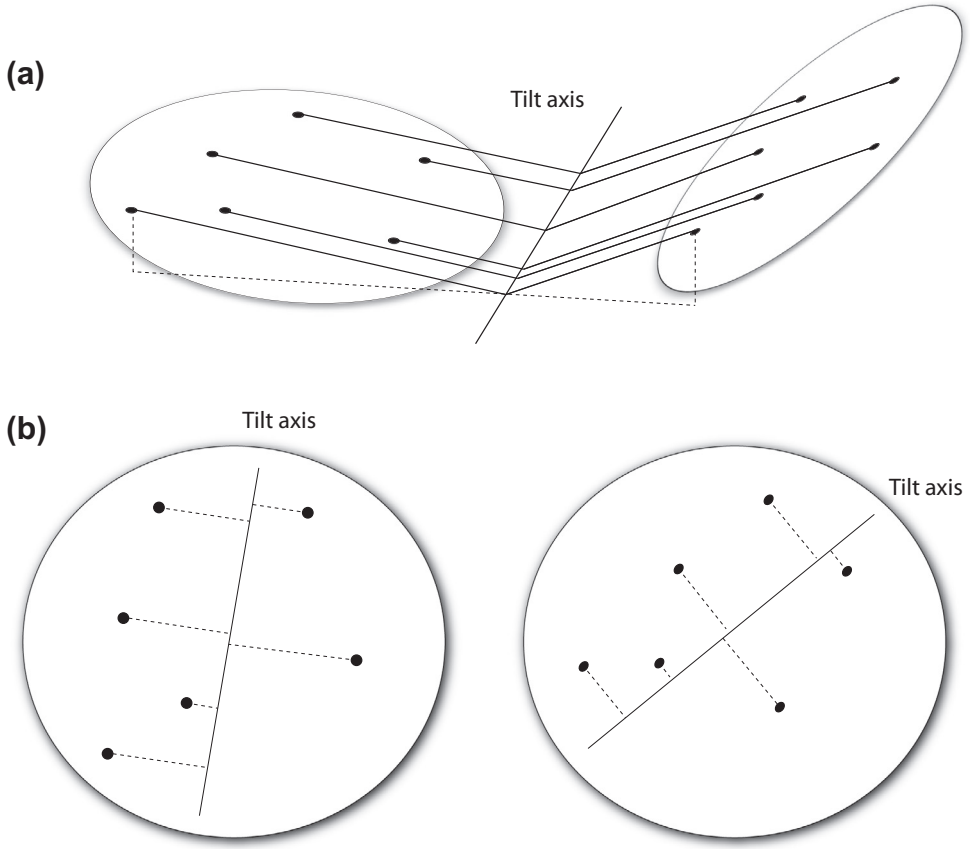


**Fig.2.** The principle of determining the orientation of the tilt-axis. (a) A sample tilted around a fixed axis has identical 1D vectors projected onto the tilt-axis. (b) Given two EM images with identified corresponding particles we search for the direction of the tilt-axis by sampling 360 × 180 possible angles. The most similar 1D projections provide the estimated tilt-axis directions. Similarity is measured as described in the text and defined in Box 1 line 4.6.

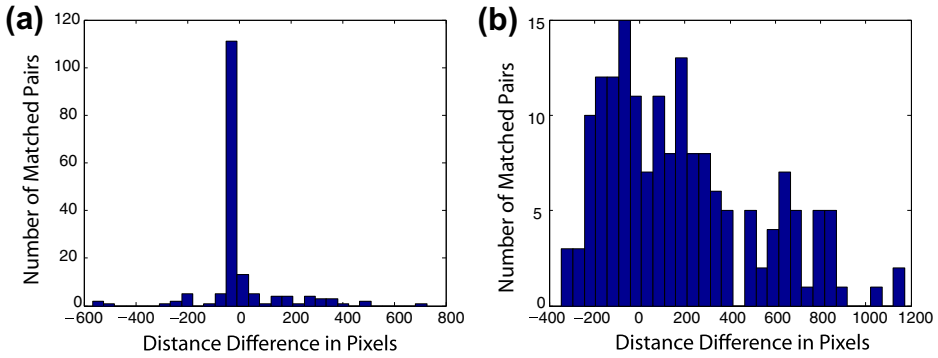


**Fig.3.** Histogram of distance differences (*x*-axis). *Y*-axis corresponds to the number of particle pairs. (a) Optimal orientation of 1D projections. More than 100 pairs contribute to the peak. Those values that lie off the main peak correspond to wrongly matched particle pairs, which will be removed. (b) Histogram of distance differences taken from an arbitrary chosen pair of angles. The main peak gives only fifteen pairs.

Our goal is to find a pair of angles under which 1D projections are most similar to each other. Luckily, since we are dealing with a relatively small number of 1D coordinate vectors we can achieve high precision if we just exhaustively sample all combinations of 360 × 180 angle pairs. Such sampling guarantees half-degree accuracy for tilt-axis estimation (Box 1: lines 4.1–4.2). To measure the similarity of 1D projections there is one unknown parameter left – the relative shift. If the correspondence between the matched particles was computed perfectly in the previous step, then we could just apply least square fitting to find both the shift and the similarity of the projections. However, outliers, i.e., wrongly matched particles, will bias the shift, and the similarity will be inaccurate. To solve both problems of outliers and relative shift we deployed the following approach, which is similar to the voting process in the Hough transform (Duda and Hart, 1972). Given two 1D projections of matched particles $\{v_i, u_i\}$ we compute their coordinate differences: $\{v_i - u_i\}$ (Box 1: line 4.3). Each such difference defines a potential shift between the projections. Correctly matched pairs are going to have similar differences. Then, we find the peak, i.e., the largest cluster, in the histogram of the differences (Fig. 3). Those difference values that lie outside of the largest peak correspond to the wrongly matched particles and are thus thrown

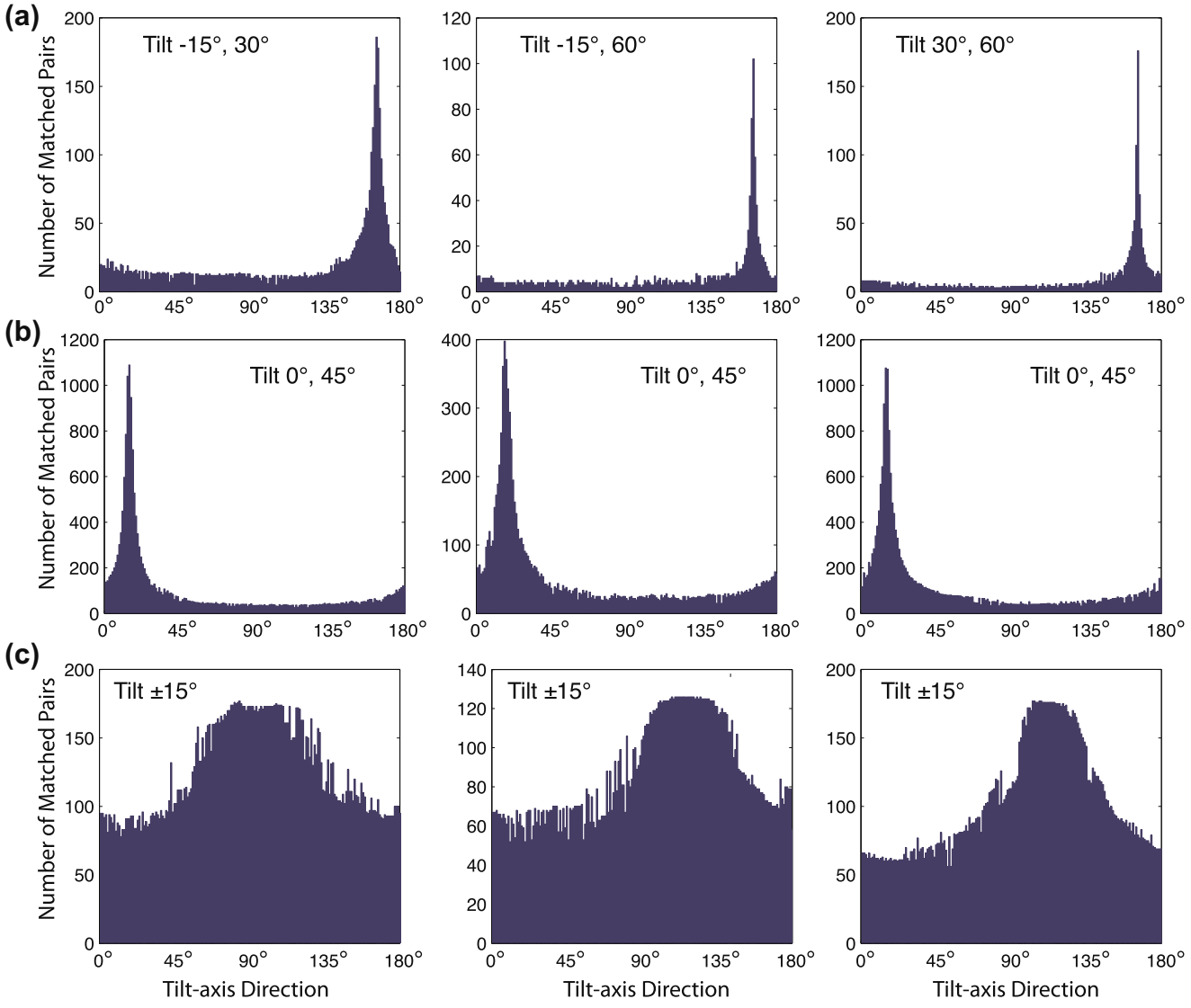


**Fig.4.** The plots display the number of detected corresponding particle pairs (*y*-axis) as the function of direction of the tilt-axis (*x*-axis). Three samples are shown for each of the following sets: (a) gold particles data set, (b) IMP dehydrogenase, (c) ribosomal data set. Notice sharp peaks, i.e., global maxima, for sets (a) and (b), but there is no sharp peak for the set (c) recorded at symmetrical angles ±15°.

away. The largest peak sampled over $360 \times 180$ angles gives the refined set of matched particles and the best estimate of tilt-axis directions (Box 1: lines 4.4–4.8). Fig. 4 demonstrates on three experimental data sets how the number of detected matched particle pairs changes as the function of the estimated tilt-axis direction.

## 4. Results

To demonstrate the performance of the PCT method we first provide results of the particle correspondence detection on two experimental data sets. We found that the accuracy of our automated method is close to the accuracy of manual picking by one of us (BGH). Next, we compared the PCT method to the affine transform in identification of tilt-axis direction. We used four types of synthetic data that modeled flat image, parabola, paraboloid and saddle. In addition, to model deviations from the ideal conditions when an EM grid is inserted into a microscope holder, we applied a small pre-tilt angle to the synthetic data sets. Finally, we analyzed the result of the tilt-axis detection on experimental data sets and discuss the benefits and limitations of the PCT method.

### *4.1. Accuracy of automated particle correspondence from experimental images*

We applied the PCT method on two experimental data sets, seven micrograph pairs with IMP dehydrogenases, and 34 micrograph pairs with *E. coli* 70S ribosomes. To estimate the accuracy we compare the results of our method to the results obtained by manual selection of particle pairs using the XMIPP software. We call the latter data the ground truth. BGH had not seen the results of the automated method at the time of particle selection. The metric that is used for the evaluation is Precision–Recall curve (Precision = True Positives/Positives, Recall = True Positives/(True Positives + False Negatives)). We produce a Precision–Recall curve parameterized by the confidence of the detections. As summary statistics, we report (1) Recall and Precision at the point of maximal *F*-measure on the curve ($F = 2 * P * R/(P + R)$), (2) average

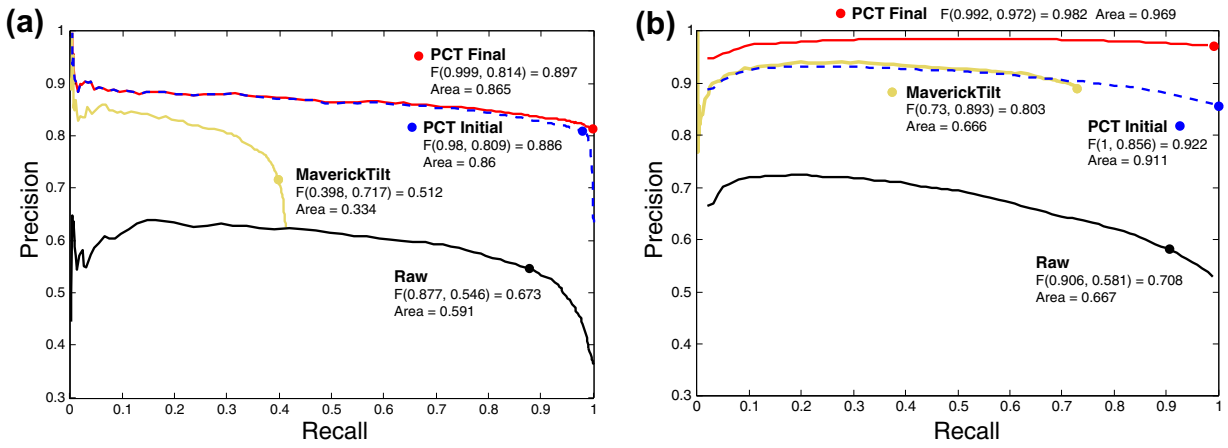


**Fig.5.** Precision-recall curves that measure the accuracy of automatic detection of corresponding particle pairs in tilted images with (a) IMP dehydrogenase particles and (b) ribosomal particles. Raw – application of TextonSVM individually on each image and not attempting to find the corresponding particle pairs. MaverickTilt – application of MaverickTilt (Hauer et al., 2013) on the Raw data set. PCT Initial – initial correspondence as found by our method (Box 1: lines 3.1–3.6) starting from the Raw data set. PCT Final – final correspondence as found by our method. Precision = True Positives/Positives, Recall = True Positives/(True Positives + False Negatives). *F* reports the summary statistics of Recall and Precision at the point of maximal *F*-measure on the curve ($F = 2 * P * R/(P + R)$). *Area* gives the area under the curve.

Precision, the area under the PR curve. Fig. 5 shows four curves for the two data sets. The curves labeled Raw are the results from running TextonSVM individually on each image and not attempting to find the corresponding particle pairs. In this case the Positives and Negatives of single particle results are defined based on the joint collection of individual particles from the ground truth set of pairs. As can be seen from the Fig. 5 (black curves) the performance is far from optimal, mostly due to many particles detected in one image but not visible in the other because the fields did not fully overlap, due to the tilt. The purpose of this experiment is to show what is the initial composition of the particles that the PCT method starts to work with (Box 1: lines 1.1–1.5). The blue curve (Fig. 5) corresponds to the results of the initial matching (Box 1: lines 3.1–3.6). There is a significant improvement but the results still might contain a portion of wrongly matched particles that, in addition, introduce errors to the estimation of the tilt-axis direction. Finally, by applying our complete algorithm, we increase both recall and precision (Fig. 5, red curve). The most apparent improvement is observed for the ribosomal data set where we recover 99% of the ground truth particles with just 3% false positives (Fig. 5(b), red curve). For the comparison, we also include results (Fig. 5 yellow curves) of MaverickTilt (Hauer et al., 2013), a recently introduced software program for matching particle pairs from a pair of tilted images.

### *4.2. Robustness of the tilt-axis estimation and comparison to the affine transform approach*

We start by demonstrating on experimental images that the affine transform cannot properly align corresponding particles from tilted image pairs if an EM grid is not perfectly flat. From the data set with gold particles we selected a tilted pair of images at 0° and 60°. We then computed an affine transformation based on the corresponding particle pairs detected by the PCT method and applied this transformation to superimpose particles relative to each of the images. If the affine transform was enough to capture the relative locations between the corresponding particles, then applying the transformation on the particles from the second image would place them directly on top of the corresponding particles from the first image. However, as shown in Fig. 6(a), the particles in the left bottom region are not co-aligned, while most of the other particles are co-aligned very tightly. This demonstrates that the affine

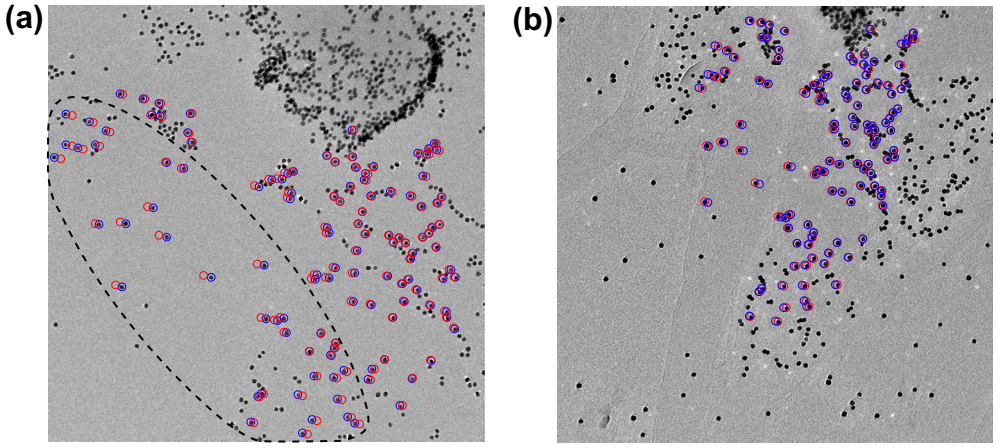


**Fig.6.** Pair of images with gold particles tilted at (a) zero and (b) 60°. Blue and red circles show matched particles for the first and second image, respectively. Circles from the other image are placed based on affine transform. Notice that, because of affine transform limitations to account for geometrical deformations of the samples, in image (a) circles in the marked region are less co-aligned than other circles.

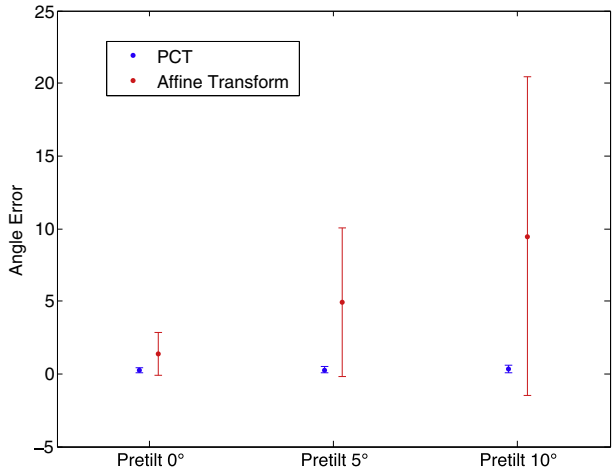


**Fig.7.** Errors of estimated tilt-axis directions for the synthetic data representing a plate with a parabolic curvature. The plate is pre-tilted at 0°, 5° and 10° (*x*-axis). The *y*-axis indicates the scale of errors in degrees from the correct tilt-axis direction. Blue corresponds to the PCT method, while red corresponds to the affine transform. For each method we plot the mean error and its standard deviation. See *Fig.* S1 for more information. (For interpretation of the references to color in this figure legend, the reader is referred to the web version of this article.)

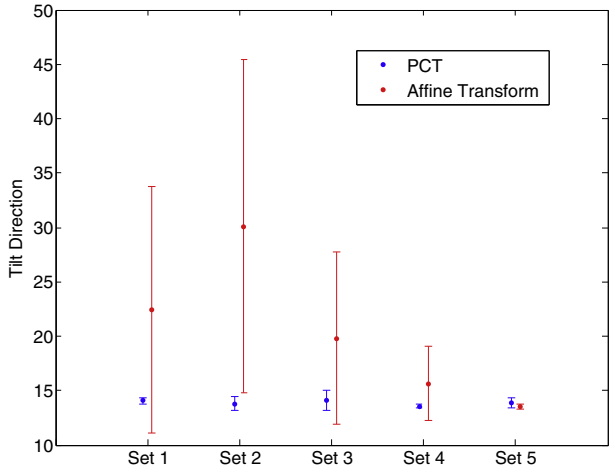


**Fig.8.** Tilt-axis direction (*y*-axis) for gold particle images (*x*-axis) is calculated by the PCT method (blue color) and by the affine transform (red color). Calculation is performed for each of the five images paired with the other four, i.e., in Set-1 the first image is paired with other four images. Mean value is plotted as a dot and variance as a bar. (For interpretation of the references to color in this figure legend, the reader is referred to the web version of this article.)

transform approach has limitations to account for geometrical distortions of EM grids.

Next, we show that even at modest deviations from perfect conditions, the commonly used affine transform makes significant errors in the estimation of the tilt-axis direction. We use four synthetic pairs of images that correspond to specimens that are perfectly flat, curved as a parabola, as paraboloid and as a saddle, respectively. Although we benchmark our approach and the affine transform in the case when the particle correspondence is perfectly accurate, noise is introduced to the particle coordinates as described above. Fig. 7 shows errors that occurred when the affine transform was used in the case of the specimen plate curved as a parabola. We pre-tilt a simulated EM grid by 0°, 5° and 10°. Fig. S1 provides more detailed information as well as additional examples for pre-tilted flat, parabaloid and the saddle types of distortions. The affine transform errors can be as high as 5° in zero pre-tilt, and as high as 15° in 5° pre-tilt cases. On the other hand, the accuracy of our method is within 2°, and, in the majority of the cases, the error is below half a degree.

### 4.3. Estimation of tilt-axis direction in experimental images

For the experimental images of gold particles and ribosomes, we do not know the true orientation of the tilt-axis. Since the gold-particle images were recorded by a CCD camera, however, there was no (small, random) rotation of the detector from one image to the next, as there might be when film is used. Therefore we presume that goniometer direction was relatively constant and there should be little difference in tilt-axis direction between all images. Fig. 8 shows five sets of the results of the estimated tilt-axis direction computed by the PCT method and by the affine transform. Each set of the results represents a pairing of one of the five images, recorded at −15°, 0°, 15°, 30° and 60°, with the other four. As it can be seen from Fig. 8, the angle of the tilt-axis that is computed by our method is almost constant at roughly 14°. One of us (DT) performed an independent estimation of the tilt-axis direction using a manual approach (unpublished) and obtained 14.5°. The affine transform, on other hand, produced an accurate result only for one set, where the image obtained at 60° tilt was paired with the other four (Fig. 8).

Images of *E. coli* 70S ribosomes were recorded from the symmetrically tilted specimens at ±15°. If the EM grid were perfectly planar and there were no pre-tilt to the sample, then the distances between the particle centers have to be identical in both images. Hence, the tilt-axis direction cannot be uniquely determined by the proposed method nor by the affine transform. Indeed, we observe that the number of detected corresponding particle pairs as the function of direction of the tilt-axis has no sharp peak (Fig. 4(c)). The width of the peak is roughly 20°. It demonstrates that there are some deviations from the perfect planarity and/or non-zero pre-tilt to the sample; however, the sharpness of the peak is not sufficient enough to accurately estimate the direction of the tilt. Indeed, our results produced relatively non-stable values as shown in (Fig. S3-a). It should be noted, that the non-uniqueness of the tilt-axis direction has, however, no effect on the accuracy of the detection of corresponding particle pairs. If the method is applied to a pair of identical images then the tilt-axis direction is going to be an arbitrary angle but exactly the same for both images. That is exactly the case for our method (Fig. S4-a); results from the affine transform, however, produce much larger differences (Fig. S4-b).

Fig. S3-b shows results of tilt-axis direction estimation for IMP dehydrogenase data set. In this case, the affine transform produced slightly more stable results (17.3° ± 0.6°) than our method (16.9° ± 1.4°).

We also applied the CTFTILT (Mindell and Grigorieff, 2003) program to calculate tilt-axis directions for the three experimental data sets (Fig. S5–7). As expected, for the non-tilted or low-angle, ±15°, tilt images the results are significantly off compared to the expected values due to the non-sufficient variation in CTF across the images. In the case of the IMP dehydrogenase images tilted at +45° the CTFTILT results match both the affine transform and our results based on the projection matching.

## 5. Implementation details

The PCT method is implemented in Matlab and the source code is available at http://www.eecs.berkeley.edu/Research/Projects/CS/vision/bioimages/. There are only a few parameters that are required to be set by the user: (1) tilt angle for each of the two images, (2) approximate particle size, and (3) size of a box to define a particle neighborhood, which depends on particle density of a

micrograph; roughly it should cover 5–20 particles. In addition, the most important input from the user is to select a few exemplars of correct particles and of the background. This is required for the application of TextonSVM method to detect particles in both images. This step can conveniently be performed through the interactive process implemented in Matlab. After applying TextonSVM the next step is the detection of corresponding particle pairs and tilt-axis directions. If desired the user can remove or add particles through the provided interactive interface.

We measured the running times of the PCT method on the IMP dehydrogenase data set (image size 2500 × 3466 pixels) using Intel Xeon X3450 2.67 GHz processor utilizing only one core. The training stage of TextonSVM based on exemplars took ~24 h. The application of TextonSVM to compute a probability map of an individual image took ~10 min per image. Computing neighborhood descriptors (Box 1 : part 2) took ~4 h per image. Finding particle correspondence (Box 1 : part 3 and 4) took ~5 h per image pair. If a user limits the search within 20° around an estimated tilt-axis direction, then the running times drop to ~30 min per image to compute neighborhood descriptors and to ~7 min per image pair to compute particle correspondence.

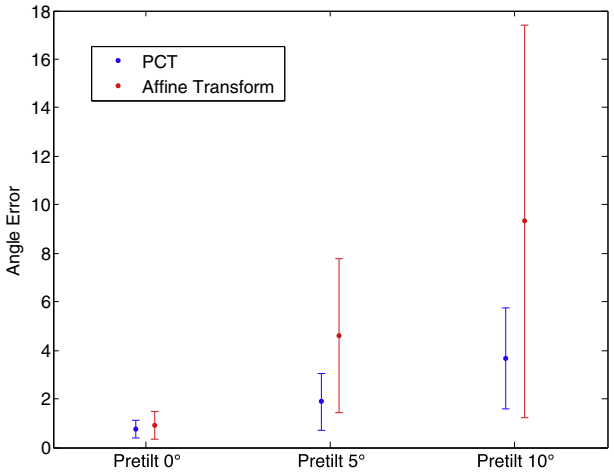


**Fig.9.** Effect of the simulated beam induced movement on estimation of tilt-axis directions. Parabolic transformation was applied to a synthetic image to mimic a beam induced movement. Errors of estimated tilt-axis direction are shown for the PCT method (blue) and for the affine transform (red). The plate is pre-tilted at 0°, 5° and 10° (*x*-axis). The *y*-axis indicates the scale of errors in degrees from the correct tilt-axis direction. See *Fig.* S2 for more information. (For interpretation of the references to color in this figure legend, the reader is referred to the web version of this article.)

## 6. Discussion

Currently, identification of corresponding particle pairs in tilted-image pairs is a semi-automated process that still requires extensive effort from a user. Automated particle picking, however, is challenging even for single images (Zhu et al., 2004). Packages like XMIPP (Scheres et al., 2008) and SPIDER (Shaikh et al., 2008) allow only manual particle pairing for tilted images. The TiltPicker program (Voss et al., 2009) provides a semi-automated solution that simplifies particle boxing and pairing. Still, picking and verifying hundreds and thousands of particles is time-consuming. While it may be very hard to devise a completely automated particle-picking program that requires zero input from the user, a reasonable balance between user effort and program accuracy is possible. In this manuscript, we applied the semi-automated approach TextonSVM, which can reduce the manual component of the particle picking process to the selection of exemplars from just one micrograph. The following step, particle correspondence in a pair of images, is performed completely in automated manner. We have shown that our automated particle correspondence method performs with high accuracy and outperforms the recently introduced method MaverickTilt (Hauer et al., 2013). Our particle correspondence method is also equally accurate in the case of symmetrical tilt, like the described above case of 70S ribosomal particles tilted at ±15°, even though our method does not uniquely determine the direction of the tilt-axis.

The second goal of this paper was to devise a computational approach that avoids possibly erroneous assumptions about EM grid geometry during the collection of tilted-image pairs. The first assumption used in the previously published methods is that the EM grid is perfectly planar. However, specimen wrinkling does happen (Vonck, 2000) and, even though the curvature angle might be small, it significantly affects the estimation of goniometer geometry if the affine transform is used for computation. The second assumption that causes the affine transform to produce erroneous results is that the goniometer axis is the single tilt-axis, i.e., that at zero-tilt the EM grid is absolutely parallel to the imaging plane. However, the specimen sample could be slightly pre-tilted in an arbitrary direction when inserted into a microscope holder. Fig. 7 shows that a pre-tilt of even 5° has a detrimental effect on affine transform results. In the case of symmetrical tilt, neither our method nor the affine transform approach are applicable to accurately compute the tilt-axis direction. If the tilt angle is large enough, CTFTILT (Mindell and Grigorieff, 2003) may be used to determine the tilt-axis.

The electron beam of a microscope can cause some areas of a sample to move during the sample acquisition (Henderson, 1992; Glaeser, 2008; Brilot et al., 2012; Bai et al., 2013). This so-called beam-induced movement causes geometrical deformations to a sample that may differ from one area of the specimen to another. Consequently, the process of sample tilting can no longer be described as a perfect rotation, and possibly a shift, of a rigid object in the three-dimensional space. This impacts the accuracy of the PCT method since our fundamental assumption is that the sample is a rigid three-dimensional object that has no internal deformations between the two image acquisitions. The differences in the tilt-axis direction of up to 2° that were estimated for the experimental particles could thus be caused by beam induced movement. Fig. 9 demonstrates that a simulated plate wrinkle of mere 4° can cause errors within a range of 3° for the tilt-axis estimation. We note, though, that the errors of the affine transform are significantly larger. We anticipate, however, that with the advancement of direct electron detectors (Bai et al., 2013) the problem of the beam induced translational movement is going to be significantly reduced.

The principle of common lines is at the core of many methods used in single particle and electron tomography. In our approach, particle correspondence and tilt-axis direction estimation are integrated into one computational scheme based on the common line principle. While, theoretically, 1D common line similarity search is sound, there potentially exists the same drawback as in volume reconstruction by angular reconstitution, where particle images are assigned Euler angles based on common line similarity. Since in the common line approach, 2D information is reduced to a 1D vector, the drawback is sensitivity to noise and lower discrimination power over 2D methods. To avoid these problems, we are not projecting the whole micrograph onto a 1D vector, but rather only detected particle centers are projected. The low density of particles relative to image size allows reliable discrimination of correct angle among the sampled 1D projections.

The RCT and OTR methods allow one to obtain a medium resolution model in a relatively short amount of time (Han et al., 2009). As the "free-hand" method (Rosenthal and Henderson, 2003) is

increasingly used with cryo frozen samples, we anticipate that small tilt angle cryo-EM will become more popular as the community heads toward unbiased and higher resolution models. Therefore, the need for software that automates particle picking and particle correspondence in tilted images will likely grow.

## Acknowledgments

We thank Florian Hauer and Holger Strak for providing program MaverickTilt. This work conducted by ENIGMA – Ecosystems and Networks Integrated with Genes and Molecular Assemblies (http://enigma.lbl.gov), a Scientific Focus Area Program at Lawrence Berkeley National Laboratory, was supported by the Office of Science, Office of Biological and Environmental Research, of the US Department of Energy under Contract No. DE-AC02-05CH11231.

## Appendix A. Supplementary data

Supplementary data associated with this article can be found, in the online version, at http://dx.doi.org/10.1016/j.jsb.2014.03.017.

## References

Arbeláez, P., Han, B.-G., Typke, D., Lim, J., Glaeser, R.M., Malik, J., 2011. Experimental evaluation of support vector machine-based and correlation-based approaches to automatic particle selection. J. Struct. Biol. 175 (3), 319–328.

Bai, X., Fernandez, I.S., McMullan, G., Scheres, S.H., 2013. Ribosome structures to near-atomic resolution from thirty thousand cryo-EM particles. ELife, 2.

Belnap, D.M., Olson, N.H., Baker, T.S., 1997. A method for establishing the handedness of biological macromolecules. J. Struct. Biol. 120, 44–51.

Brilot, A.F., Chen, J.Z., Cheng, A., Pan, J., Harrison, S.C., Potter, C.S., Carragher, B., Henderson, R., Grigorieff, N., 2012. Beam-induced motion of vitrified specimen on holey carbon film. J. Struct. Biol. 177, 630–637.

Cheng, N., Trus, B.L., Belnap, D.M., Newcomb, W.W., Brown, J.C., Steven, A.C., 2002. Handedness of the herpes simplex virus capsid and procapsid. J. Virol. 76, 7855–7859.

Duda, R.O., Hart, P.E., 1972. Use of the Hough transformation to detect lines and curves in pictures. Commun. ACM 15 (1), 11–15.

Frank, J., 2006. Three-Dimensional Electron Microscopy of Macro-molecular Assemblies: Visualization of Biological Molecules in Their Native State. Oxford University Press, New York.

Glaeser, R.M., 2008. Retrospective: radiation damage and its associated 'Information Limitations'. J. Struct. Biol. 163 (3), 271–276.

Glaeser, R.M., Downing, K.H., DeRosier, D., Chiu, W., Frank, J., 2006. Electron Crystallography of Biological Macromolecules. Oxford University Press, New York.

Han, B.-G., Dong, M., Liu, H., Camp, L., Geller, J., Singer, M., Hazen, T.C., Choi, M., Witkowska, H.E., Ball, D.A., Typke, D., Downing, K.H., Shatsky, M., Brenner, S.E., Chandonia, Biggin, M.D., Glaeser, R.M., 2009. Survey of large protein complexes in *D. vulgaris* reveals great structural diversity. Proc. Natl. Acad. Sci. USA 106 (39), 16580–16585.

Hauer, F., Gerle, C., Kirves, J.-M., Stark, H., 2013. Automated correlation of single particle tilt pairs for random conical tilt and orthogonal tilt reconstructions. J. Struct. Biol. 181 (2), 149–154.

Henderson, R., 1992. Image contrast in high-resolution electron microscopy of biological macromolecules: TMV in ice. Ultramicroscopy 46 (1–4), 1–18.

Henderson, R., Chen, S., Chen, J.Z., Grigorieff, N., Passmore, L.A., Ciccarelli, L., Rubinstein, J.L., Crowther, R.A., Stewart, P.L., Rosenthal, P.B., 2011. Tilt-pair analysis of images from a range of different specimens in single-particle electron cryomicroscopy. J. Mol. Biol. 413, 1028–1046.

Leschziner, A., 2010. Chapter nine – the orthogonal tilt reconstruction method. In: Jensen, Grant J. (Ed.), Methods in Enzymology. Academic Press, pp. 237–262, Vol. 482.

Leschziner, A.E., Nogales, E., 2006. The orthogonal tilt reconstruction method: an approach to generating single-class volumes with no missing cone for ab initio reconstruction of asymmetric particles. J. Struct. Biol. 153 (3), 284–299.

Mindell, J.A., Grigorieff, N., 2003. Accurate determination of local defocus and specimen tilt in electron microscopy. J. Struct. Biol. 142 (3), 334–347.

Penczek, P.A., Grassucci, R.A., Frank, J., 1994. The ribosome at improved resolution: new techniques for merging and orientation refinement in 3D cryo-electron microscopy of biological particles. Ultramicroscopy 53 (3), 251–270.

Radermacher, M., 1988. Three-dimensional reconstruction of single particles from random and nonrandom tilt series. J. Electron Microsc. Tech. 9, 359–394.

Radermacher, M., Wagenknecht, T., Verschoor, A., Frank, J., 1986. A new 3-D reconstruction scheme applied to the 50S ribosomal subunit of *E. coli*. J. Microsc. 141 (1), RP1–RP2.

Rosenthal, P.B., Henderson, R., 2003. Optimal determination of particle orientation, absolute hand, and contrast loss in single-particle electron cryomicroscopy. J. Mol. Biol. 333 (4), 721–745.

Scheres, S.H.W., Núñez-Ramírez, R., Sorzano, C.O.S., Carazo, J.M., Marabini, R., 2008. Image processing for electron microscopy single-particle analysis using XMIPP. Nat. Protoc. 3 (6), 977–990.

Scheres, S.H.W., Melero, R., Valle, M., Carazo, J.-M., 2009. Averaging of electron subtomograms and random conical tilt reconstructions through likelihood optimization. Structure 17 (12), 1563–1572.

Shaikh, T.R., Gao, H., Baxter, W.T., Asturias, F.J., Boisset, N., Leith, A., Frank, J., 2008. SPIDER image processing for single-particle reconstruction of biological macromolecules from electron micrographs. Nat. Protoc. 3 (12), 1941–1974.

Tang, G., Peng, L., Baldwin, P.R., Mann, D.S., Jiang, W., Rees, I., Ludtke, S.J., 2007. EMAN2: an extensible image processing suite for electron microscopy. J. Struct. Biol. 157, 38–46.

Typke, D., Nordmeyer, R.A., Jones, A., Lee, J., Avila-Sakar, A., Downing, K.H., Glaeser, R.M., 2005. High-throughput film-densitometry: an efficient approach to generate large data sets. J. Struct. Biol. 149 (1), 17–29.

Van Heel, M., 1987. Angular reconstitution: a posteriori assignment of projection directions for 3D reconstruction. Ultramicroscopy 21 (2), 111–123.

Vonck, J., 2000. Parameters affecting specimen flatness of two-dimensional crystals for electron crystallography. Ultramicroscopy 85, 123–129.

Voss, N.R., Yoshioka, C.K., Radermacher, M., Potter, C.S., Carragher, B., 2009. DoG Picker and TiltPicker: software tools to facilitate particle selection in single particle electron microscopy. J. Struct. Biol. 166 (2), 205–213.

Zhu, Y., Carragher, B., Glaeser, R.M., Fellmann, D., Bajaj, C., Bern, M., Mouche, F., de Haas, F., Hall, R.J., Kriegman, D.J., Ludtke, S.J., Mallick, S.P., Penczek, P.A., Roseman, A.M., Sigworth, F.J., Volkmann, N., Potter, C.S., 2004. Automatic particle selection: results of a comparative study. J. Struct. Biol. 145 (1–2), 3–14.